BioNanoScience (2024) 14:457–473
https://doi.org/10.1007/s12668-023-01238-3

Catalytic, Antioxidant, and Antifungal Applications of ZnO Nanoparticles: Facile Green Synthesis by *Crataegus oxyacantha* Leaf Aqueous Extract

Alireza Momeni[1] · **Mohammad Hadi Meshkatalsadat**[1] · **Behjat Pouramiri**[1]

Accepted: 2 November 2023 / Published online: 16 November 2023

Abstract

The present study describes facile and uncomplicated biosynthesis of ZnO nanoparticles (NPs) using leaf extract of *C. oxyacantha*. The biomolecules present in the leaf extract act as capping agents. Thus, hazardous chemical agents are eliminated in this green synthesis. The exclusivity of biosynthesized ZnO NPs was investigated through UV–VIS spectrum, FT-IR, XRD, FE-SEM, and BET. In addition, the catalytic and biomedical applications of ZnO NPs were estimated thorough several studies including organic dye degradation by ZnO nanocatalyst and photo-nanocatalyst, Suzuki cross-coupling reaction photocatalysis in producing biphenyl, antioxidant, and antifungal activity. The biosynthesized ZnO NPs have a hexagonal wurtzite structure with an average grain size of 28.68 nm, and particles in range of 20 to 70 nm and spherical structure according to XRD and FE-SEM analyses. The ZnO photo-nanocatalyst with specific band gap of 2.63 eV could degrade methylene blue under UV light and sunlight in 20 and 50 min, respectively, and successfully photocatalysis the Suzuki cross-coupling reaction in production of biphenyl under LED light. Also, ZnO NPs decolorized the organic dye in 5 min after reducing methylene blue with $NaBH_4$. By comparison to ascorbic acid, ZnO NPs were more effective at scavenging unstable DPPH at 200 μg mL^{-1}, and analyzing the MIC and the inhibition zone against *Aspergillus niger* and *Aspergillus brasiliensis*, ZnO NPs were shown to be effective in inhibition of these microbes while the *C. oxyacantha* leaf extract did not inhibit any microbial growth.

Keywords Antifungal · Antioxidant · Green synthesis · Nanocatalyst · Suzuki coupling · ZnO nanoparticles

Abbreviation

BET	Brunauer-Emmett-Teller
CLSI	Clinical & Laboratory Standards Institute
DPPH	2,2-Diphenyl-1-picryl-hydrazyl-hydrate
FT-IR	Fourier-transform infrared spectroscopy
IUPAC	International Union of Pure and Applied Chemistry
MB	Methylene blue
NPs	Nanoparticles
ROS	Reactive oxygen species
SEM	Scanning electron microscope
UV-Vis	Ultraviolet–visible spectroscopy
XRD	X-ray diffraction
ZnO	Zinc oxide

✉ Mohammad Hadi Meshkatalsadat
meshkatalsadat.m@qut.ac.ir

Alireza Momeni
momeni.a@qut.ac.ir

Behjat Pouramiri
b.pouramiri.chem@gmail.com

[1] Department of Chemistry, Qom University of Technology, Qom, IR, Iran

1 Introduction

Nanotechnology, as a cutting-edge technology with numerous applications, has now become a widely recognized state-of-the-art technology. Nanoparticles (NPs) are rapidly becoming the subject of interest in the fields of engineering, biomedicine, and bioremediation. The most commonly used nanomaterials include metals, metal oxides, carbon nanotubes, nanographenes, and nanocomposites, which can be produced with varying degrees of specificity using different methods. In the last few years, large-scale applications featuring metals and metal oxide nanoparticles have become popular [1, 2]. The use of ZnO NPs has gained much attention among metal oxide nanoparticles. In addition to their chemical stability and nontoxicity, these materials are also versatile and can be used in biosensing, drug delivery,

tissue engineering, catalytic activity, and some other scientific fields owing to their optimal surface-to-volume ratio [3].

Both top-down and bottom-up methods can be used to fabricate nanostructured substances. The bottom-up method requires nanostructures to be assembled layer-by-layer [4]. Atoms, ions, and molecules can be chemically reacted to form nanoparticles in the bottom-up method [5]. As an alternative, top-down approaches must reduce the scale down to nanometers with feasible methods such as cutting, picking, chopping, and crushing [6]. By using a bottom-up approach, scientists can manipulate the shape and dimensions of nanoparticles, which is a significant benefit. Therefore, chemicals and biological products are the main components of bottom-up synthesis [7, 8]. As a novel bottom-up approach, green synthesis of nanoparticles is an environmentally friendly and non-toxic process in which the main reaction occurring is reduction/oxidation. The phyto-synthesis technique is an easy means to replace chemical and physical methods since it is low-cost and does not use toxic chemicals [9]. Plants, bacteria, fungi, and algae can contribute to green synthesis. Biogenic synthesis eliminates pollution and its destructive effects on the environment and in addition allows large-scale production of ZnO nanoparticles [10]. Plants are the most suitable source to fabricate nanostructures, as they can produce large-scale, stable nanoparticles in a variety of shapes and sizes. While different parts of plants have been used to synthesize nanoparticles, leaves have been most commonly used due to their availability and easy extraction method [11].

Phytochemicals such as alkaloids, tannins, terpenoids, and flavonoids, which are secondary metabolites found in plants, possess antimicrobial properties [12]. *Crataegus oxyacantha*, too, contains many active ingredients, including oligomeric procyanidins flavonoids, triterpenic acids, phenolic acids, fatty acids, triterpenes, sterols, and phenol carboxylic acids [13]. Also, both the leaves and fruit of the *C. oxyacantha* tree are rich in polyphenols including epicatechin, quercetin, quercetin-3-o-b-glucoside, quercetine-3-rutinoside, naringenin, caftaric acid, and caffeic acid [14].

Two common fungi, *Aspergillus niger* and *Aspergillus brasiliensis*, are excellent candidates for in vitro antifungal trials. As an important cosmopolitan fungus for postharvest decay of different substrates, *A. niger* (black mold) is a filamentous ascomycete with rapid growth characteristics and pH tolerance that is relatively high. This fungus can be found almost everywhere on the planet, including soil, water, decaying plant matter, and many types of food and feed. Furthermore, *A. niger* is among the identified fungi as GRAS (generally recognized as safe) by FDA. In spite of the safe classification, it was found that *A. niger* is an opportunistic cause of human infections. It is extremely dangerous if inhaled in sufficient quantities. Furthermore, it results in huge economic losses due to its association with various plant diseases. Alongside animal and plant pathogens, there are also reports that it produces toxic compounds including ochratoxin A, fumonisin B2, and aflatoxins in stored commodities, which seems inevitable. In addition to discoloration, quality destruction, decreased market and commercial value, *niger* mycotoxins may also cause some health issues related to the liver, kidneys, nervous system, muscles, skin, respiratory organs, digestive tract, and genital organs [15–17] As the second species, *Aspergillus brasiliensis* is a common food contaminant. It is widespread in soil and is also regularly found in indoor environments, such as industrial facilities. Human disease caused by *A. brasiliensis* is rare; however, if it occurs, it can lead to a serious lung disease called aspergillosis. Agar plates containing Sabouraud dextrose agar (SDA) can be used to detect *A. brasiliensis*. It is an opportunistic pathogen, meaning that it becomes pathogenic through a break in the first line of defense. Infections are more likely to occur in people who have a weakened immune system, whether from another illness, or who have been hospitalized for long periods of time. Aspergillosis is treated when it is confirmed with medications containing antifungal molecules, such as voriconazole and amphotericin B1 [18]. A variety of plant extracts including *Beta vulgaris*, *Cinnamomum tamala*, *Cinnamomum verum*, and *Brassica oleracea var. Italica* were utilized to synthesize zinc oxide nanoparticles by Pillai et al. [19] to asses antifungal activity against *A. niger*. Among all the prepared ZnO NPs, only *Beta vulgaris*- and *Brassica oleracea var. italica*-mediated ZnO NPs exhibited antifungal activity against *A. niger* in the aforementioned research. It is therefore crucial to evaluate the antifungal activity of nanoparticles synthesized from plant extracts. In addition to their antimicrobial properties, ZnO nanoparticles are extremely strong antioxidants, and the most common way they scavenge radicals is by producing reactive oxygen species (ROS) [20]. A variety of tests including DPPH, ABTS, and TEAC can be used to verify the antioxidant activity of biosynthesized ZnO NPs [21]. Due to the basic metabolic activities in our body, oxygen free radicals are produced as byproducts. Hence, cell membranes can be destroyed by these harmful units, DNA can be disintegrated, and the cellular enzymes can be disrupted [22]. Consequently, nanoparticles can be a significant candidate for removing or scavenging them in a safe and efficient manner with the least possible side effects.

The catalytic activity of all metal nanoparticles, such as Pd, Ag, Au, Ni, and ZnO, has been observed in a variety of reactions. A metal nanoparticle with a large surface area and many active sites is particularly useful for this purpose [23]. Therefore, we investigated three different types of catalytic reactions in order to develop novel materials. There has been much attention focused on Suzuki coupling since it became one of the most famous cross-coupling reactions in chemistry, materials, and industry. Synthetic chemistry relies heavily on Suzuki coupling for C–C bond construction, one of the most extensively studied techniques. Generally, palladium-based

catalysts have been extensively utilized for studying this reaction up to present [24]; however, our study comprise novel green and safe phyto-nanocatalyst for reaction photocatalysis. These nanomaterials are also notable for their environmental properties, known as organic dye reduction. While various industrial applications use organic cationic and anionic dyes, the process of textile dyeing wastes nearly 15% of dyes, which are discharged into the environment, and due to their endurance, they constitute a significant source of pollution [25, 26]. Methylene blue (MB), as aromatic heterocyclic and one of the most used organic dyes in textile industry, has a long history of more than 120 years utilization in biomedical applications [27]. Nevertheless, because of its substantial toxicity and the destructive effects it has on the environment, MB can cause a serious threat to human health above a specified concentration [28]. Human and animal health can be adversely affected by MB in several ways, including respiratory distress, abdominal disorders, blindness, and digestive issues [29]. Even at very low concentrations, MB in water produces highly colored products. Its high molar absorption coefficient leads to its high absorption rate (8.4×10^4 L mol^{-1} cm^{-1} at 664 nm), that by reducing sunlight transmittance, decreasing oxygen solubility, and affecting aquatic life's photosynthetic activity, and it reduces biodiversity and aesthetics [28, 30]. Utilizing metal oxide catalysts such as ZnO, and $NaBH_4$, which act as reductant agents, is a facile and effective way to degrade MB. Zinc oxide nanoparticles display a high surface-to-volume ratio and remarkable surface adsorption as an n-type semiconductor [31]. In general, photocatalytic degradation is more environmentally friendly than adsorption [32]. ZnO NPs in addition to having high redox potential, nontoxicity, and environmental friendliness, it is also low in cost and exhibit high exciton binding energy which leads to remarkable photocatalytic activity in reducing Methylene blue-contaminated water [33–35]. Moreover, it exhibits greater photocatalytic activity than TiO_2 in the photodegradation of organic pollutants due to its ability to absorb a larger fraction of the UV spectrum [36].

Thus, in the present study, we evaluated the catalytic activity of *C. oxyacantha* leaf extract-mediated ZnO NPs, as well as the antioxidant and antifungal properties through DPPH, well diffusion and minimum inhibition concentration (MIC) tests respectively. Also,UV–Vis spectra, FTIR, XRD, SEM, and BET were analyzed for the characterization of synthesized ZnO NPs.

2 Materials and Methods

2.1 Chemicals and Reagents

Fresh *C. oxyacantha* leaf was collected from Tonkabon jungle in Mazandaran province of Iran. Analytically grade metallic salt precursor, zinc sulfate ($Zn(SO_4)0.7H_2O$), NaOH (sodium hydroxide), NaBH4 (sodium borohydride), and Methylene blue purchased from Merck®, Germany, were used. Following green chemistry principles, harmful reagents were removed from the synthesis, and only water was used.

2.2 Preparing Plant Extract

Aqueous leaf extract was prepared by using the method proved by Sekhar et al. [37] which adapted slightly. Impurities were removed from the leaves by washing them twice in double-distilled water. A half-hour heating in double-distilled water over 80 °C followed the drying 20 gr of the leaves. With the use of Whatman grade No. 1 filter paper, the aqueous leaf extract was filtered after 30 min and the dark yellow hue of pure *C. oxyacantha* extract was observed. For further analysis, the filtrate extract was centrifuged at 7500 rpm for 10 min before being stored at 4 °C.

2.3 ZnO NP Biosynthesis by Green Approach

Using a simple and inexpensive method, 20 mL of fresh *C. oxyacantha* leaf extract was added drop by drop into 100 mL of continuously stirring solution containing 1.43 g $Zn(SO_4)$ at 60 °C. At a pH of 12.0 as optimum PH, the reaction was maintained until a brownish powder appeared, then washed with double-distilled water and standard ethanol to remove possible impurities, and afterwards centrifuged at 8000 rpm for 15 min. Over a period of 2 h, the precipitate was dried at around 400 °C in a hot air oven. The synthesized powder samples were utilized for further characterization. Figure 1 shows the proposed mechanism for forming green synthesized ZnO NPs.

2.4 ZnO NP Characterization

By using a Shimadzu UV-160 A series UV–VIS spectrophotometer in the range of 190–1100 nm, green synthesized ZnO NPs and leaf extract were characterized. Morphological characteristics of the surface, crystalline size, and shape of the green approach synthesized ZnO NPs was inquired by FE-SEM (TESCAN MIRA3). For a comparative analysis of the synthesized nanoparticles and leaf extract, the Fourier transform infrared (FT-IR) spectrophotometer (Perkin Elmer, Spectrum 100 series) was used, which operates in the spectral range of 4000–500 cm^{-1}. In order to determine the XRD pattern of the biosynthesized ZnO NPs, an X-ray diffractometer (XRD Philips PW1730) with wavelength of Cu Kα radiation in 2Θ range from 10 to 80° by 0.04° sec^{-1} steps was used. In addition, Microtrac Bel Corp (Belsorp mini II) was used to measure the surface area and pore size of ZnO NPs through nitrogen absorption BET.

2.5 Antioxidant Assay–DPPH Test

An effective method for measuring radical scavenging activity is to use DPPH (2,2-diphenyl-1-picrylhydrazyl). The DPPH assay uses antioxidants that react with stable DPPH* (deep violet color) and then alter it into 2,2-diphenyl-2-picrylhydrazine (DPPH:H) that shows yellow discoloration [38]. As part of the experiment, 600 µL of 1M dissolved DPPH solution dissolved in 100% methanol were added to various concentrations of ZnO NPs mediated by *C. oxyacantha* leaf extract (12.5–250 µg/mL). After vigorous shaking, 40 min of incubation in the dark was devoted to the mixture. During the study, ascorbic acid was present as a positive control. As soon as the incubation period was over, the absorbance of the reactant was measured at OD517 nm. A comparison was conducted between the DPPH scavenging activity of ZnO NPs synthesized from leaf extracts of *C. oxyacantha* and that of ascorbic acid.

Using the formula below, we derived the percentage of RSA (free radical scavenging activity):

$$\mathrm{RSA}(\%) = [(\text{A control(absorbance of DPPH without sample)} - \text{A sample(absorbance of DPPH with sample)}/\text{A control}] \times 100 \quad (1)$$

2.6 Antifungal Assay

2.6.1 Well Diffusion Test

A study was conducted on *Aspergillus niger* (ATCC 9029) and *Aspergillus brasiliensis* (ATCC 16404) to determine whether green synthesized ZnO NPs and *C. oxyacantha* leaf extract are antifungal. The antifungal activity was performed with well diffusion and MIC techniques. In the well diffusion test, which was performed according to CLSI standards [39], petri plates containing Sabouraud dextrose agar culture medium were prepared, and wells with a diameter of 6 mm were created on the culture medium. Afterward, 100 µL of 6-day-old fungi purchased from Kashan university of Iran was spread on 6-cm petri plates containing 5 ml of Sabouraud dextrose agar (SDA) culture medium (Merck®, Germany). In the next step, 10 µL (300 µg) of biosynthesized ZnO NPs and 300 µg of *C. oxyacantha* leaf extract were poured in the wells on the culture medium. Afterwards, the sterile plates were incubated at 28 ± 0.5 °C for 72 h. Nystatin ($C_{47}H_{75}NO_{17}$) served as the positive control in this assessment. As a result of the incubation, zones of inhibition were observed. This parameter was used to measure the antifungal activity of the extract and nanoparticles. With the help of ImageJ software, the diameter of the inhibition zones was measured.

2.6.2 Minimum Inhibition Concentration (MIC) Evaluation

Testing the antimicrobial activity of ZnO NPs against test pathogens was carried out using the broth dilution method [40]. The minimum inhibitory concentration of a test sample is the concentration below which the fungi will not grow. In order to determine MIC values, a range of concentrations of ZnO NPs (2–0.031 mg/mL) were tested on *A. niger* and *A. brasiliensis.* An initial concentration of 2 mg/mL was prepared from the precipitated ZnO NP samples and then diluted twofold. Test plates containing 1 mL of Sabouraud Dextrose Broth were filled with 1 mL of each nanoparticle concentration. Fungal spore suspension (3×10^3 CFU/m) made from a 5-day-old fungal culture was then injected into the plates and incubated at 25 °C for 48 h in the Bio-Oxygen Demand incubator.

2.7 Catalytic Properties of Biosynthesized ZnO NPs

The catalytic activity of ZnO NP was investigated using MB as a dyestuff model. For this purpose, $NaBH_4$ was used as a reducing agent, and the reduction was monitored with a UV–Vis spectrophotometer. We performed a model reaction by adding 100 mg of ZnO NPs to 30 mL solution of 5 mg L^{-1} Methylene blue and 120 mg $NaBH_4$. The reduction of methylene blue by ZnO NPs was investigated by recording the decrease of absorbance every 1 min by UV–VIS (Shimadzu UV-160 A) in the 200–800 nm range.

2.8 Photocatalytic Properties of Biosynthesized ZnO NPs

A facile approach, using nanocatalyst and MB dye, was employed to measure the photocatalytic activity of green synthesized ZnO NPs in an isolated box containing a 10 W UV lamp (Merck Millipore) irradiating to 30-mL glass balloon. Photocatalytic degradation was initiated by adding 100 mg of the phyto-nanocatalyst into 30 mL of an MB solution, at a concentration of 5 mg L^{-1}. The solution was stirred mechanically by cylindrical magnetic stirring bar PTFE 25 × 6 mm (Azlon®) and by measuring the UV–VIS absorption intensity in the 200–800 nm range every 5 min, the MB concentration was determined (Fig. 2).

2.9 Suzuki Cross-Coupling Photocatalytic Reaction

In the Suzuki cross-coupling reaction by ZnO nanophotocatalyst, 0.07 ml iodobenzene (Merck®-820,730), 0.5 g phenylboronic acid (Merck®-843,854) and 0.21 g potassium carbonate (Merck®-104,928) was added to

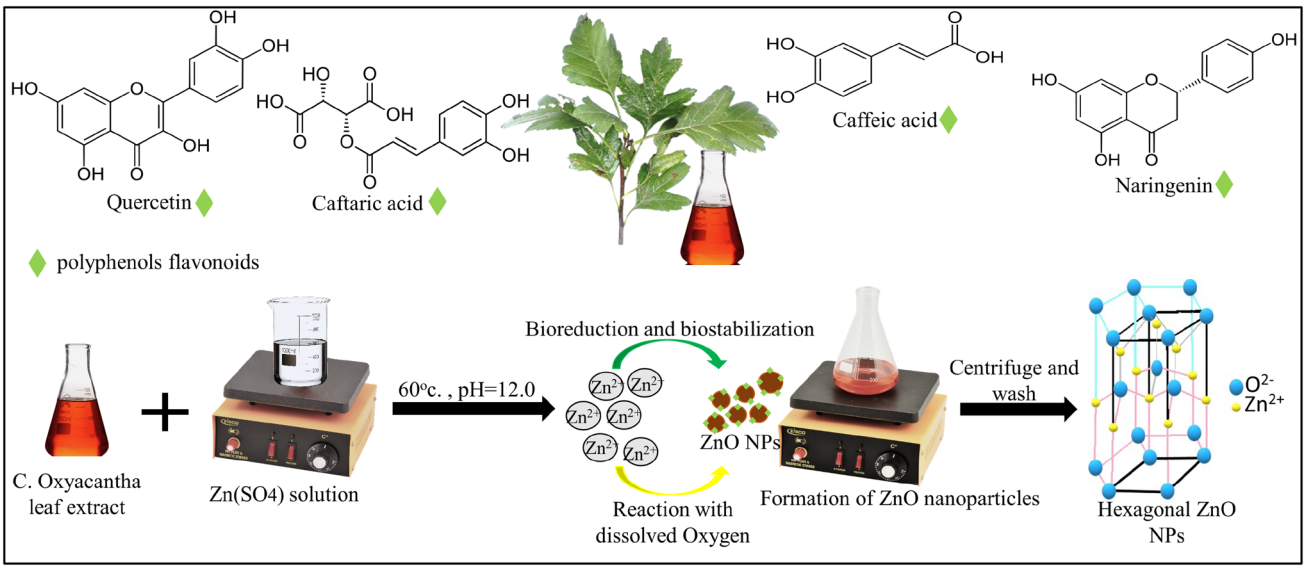

Fig. 1 Proposed mechanism of green synthesis of ZnO NPs by *C. oxyacantha* leaf extract

2-mL flask. 5 mg of biosynthesized ZnO NPs was added to the prepared mixture as photocatalyst. The mixture was stirred for 15 min under a 20-W LED lamp as light source.

Afterward, using ethyl acetate, the extraction process was done. Following the drying of the organic layer by magnesium sulfate, through slow evaporation, the ethyl acetate was removed. Chromatography was used to purify the final white solid yield. The biphenyl was characterized by IR, ^{1}H-NMR and ^{13}C-NMR and the melting temperature was determined by placing a small amount in a capillary tube and, using a thermometer in a heating bath, measuring the start and end of melting process.

3 Result and Discussion

3.1 Biosynthesized ZnO NP Characterization

3.1.1 UV–VIS and Band Gap Analysis

It was confirmed by using UV–vis spectra showing a massive peak at 386 nm that zinc ions were reduced to zinc oxide nanoparticles. However, comparison of UV–VIS spectrum of leaf extract and zinc oxide nanoparticles differentiates the formation of nanoparticles (Fig. 3a). As a result of the absorption of a photon and the excitation of an electron from the valence band into the electron/hole pair created by the conduction band, zinc oxide nanoparticles showed an absorption at 386 nm. Thereafter, by using the bandgap Tauc plot calculation, it was determined that the bandgap was 2.63 eV (Fig. 3b). Enhanced conductivity results from a decrease in the optical band gap as the absorption edge shifts towards longer wavelengths [40]. Due to their smaller band gap, biosynthesized ZnO NPs can easily be considered as photocatalysts. Such nanoparticles are capable of degrading methylene blue and other dyes due to their high photocatalytic activity. An electron in a larger band gap needs more energy to be excited from the valence band to the conduction band; by contrast, an electron in a smaller band gap can be excited easily [41]. There are many factors that influence the band gap, among which the grain size, oxygen deficiency, surface roughness, and lattice strain have the most impact [42].

3.1.2 FT-IR Analysis

The FT-IR spectrum of biosynthesized ZnO NPs and *C. oxyacantha* leaf extract are exhibited in Fig. 4. The phytochemical synthesized ZnO NPs showed a clear stretching peak at 501.03 cm^{-1} related to Zn–O formation due largely to flavonoid (polyphenol) compounds and protein molecule stabilization. The next peak at 617.78 cm^{-1} and 628.05 cm^{-1} could be appointed to C-H bending. The peaks at 1076.90 cm^{-1} carbohydrate (C-O), 1400–1488 cm^{-1} (N–H), 1617 cm^{-1} (C = N) and 3413–3549 cm^{-1} (O–H and N–H) are indicating presence of alkaloids, flavonoids derivatives, and phenolic compounds. A broad stretching band is observed at 3413, 3431, 3474, and 3549 cm^{-1}, which indicates hydrogen bonds. Changing positions or intensities of peaks in the sample spectrum can be attributed to the interaction between flavonoids and phenols and ZnO NPs. The functional groups of plant leaf extract donate reducing electrons that reduce Zn^{2+} to Zn^{1+} which changes to zinc oxide NPs. In addition, these functional groups can stabilize the ZnO formation. It

was observed that there were slight differences in peak intensities between biosynthesized zinc oxide and leaf extract in the FT-IR spectrum, which can be explained by the presence of similar biomolecules in green synthesized nanoparticles [41–43].

3.1.3 XRD Analysis

The XRD pattern of biosynthesized ZnO NPs which is exhibited in Fig. 5 presents the formation of nanocrystalline phases by well-defined broad peaks at high intensities. In accordance with Joint Committee on Powder Diffraction Standards (JCPDS) card no. 01–294 079–0205, the observed peaks demonstrate a hexagonal ZnO wurtzite-type structure. Explicit reflections at 31.94°, 34.70°, 36.47°, 47.80°, 56.76°, 63.11°, 66.65°, 68.14°, 69.32º, 72.84º, and 77.10º corresponding to (100), (002), (101), (102), (110), (103), (200), (112), (004), and (202) orientations, respectively, are shown in the figure.

In addition, ZnO NP polycrystalline structures are clearly visible in the peak at (101). Utilizing the Debye–Scherrer equation ($D = 0.9\lambda/\beta \cos \theta$), we calculated an average crystallite size of 28.68 nm for ZnO NPs. According to the calculation ZnO NP size varies from 20.51 to 52.42 nm.

3.1.4 FE-SEM analysis

The FE-SEM image exhibit spherical shape ZnO NPs with high aggregations, because of higher surface area and the durable affinity amongst them (Fig. 6). It may be argued that the stability of nanoparticles and agglomeration are strongly influenced by ecological factors. As a result, nanoparticles adhere to each other during formation and impulsively form clusters that are asymmetric [44, 45]. According to the SEM analysis, ZnO NP size mostly varies from 20 to 70 nm. In addition, the nanoparticles size range is presented in Fig. 6.

3.1.5 BET Analysis

To obtain more information about the pores in ZnO, nitrogen adsorption/desorption (BET) analysis was performed (Fig. 7a). According to IUPAC classification, the observed hysteresis loops belong to the H3 type, which shows the existence of mesoporous with 20 to 50 nm pores in ZnO NPs, by using the BJH method total pore volume and average pore diameter were calculated, which are 0.0376 $cm^3\ g^{-1}$ and 17.40 nm, respectively. According to the BJH diagram (Fig. 7b), the pore size is not uniformly distributed. The specific surface area (S_{BET}) of the ZnO powder was 8.65 $m^2\ g^{-1}$ (Table 1).

3.2 Biomedical Applications of the Biosynthesized ZnO NPs

3.2.1 Antioxidant Activity

The term antioxidant refers to substances that, even in low concentrations, significantly retard or suppress oxidation of an oxidizable substrate [46]. The physiological function of antioxidants, as suggested by this definition, is to ensure that cellular components are not damaged as a result of chemical reactions by free radicals [47]. Since antioxidants can treat a variety of illnesses, they are an essential part of human health. While several studies using standard in vitro methods have demonstrated that zinc oxide nanoparticles are potent antioxidants, biosynthesis of them by using plant extract containing flavonoids and phenols enhance the bioactivity via synergistic interaction between ZnO NPs and phytochemicals. In other words, it is likely that the antioxidant effect against radicals emanate also from electrostatically attraction of bioactive compounds (COO^-, O^-) and nanoparticles (Zn^{2+} and O_2^-) to each other, due to their negatively and positively charged electrons [48]. Research by Mehran Alavi et al. [49] shows that ZnO nanoparticles had more ability of radical scavenging than *Artemisia haussknechtii* leaf extract which contain phenolic and flavonoids combination,

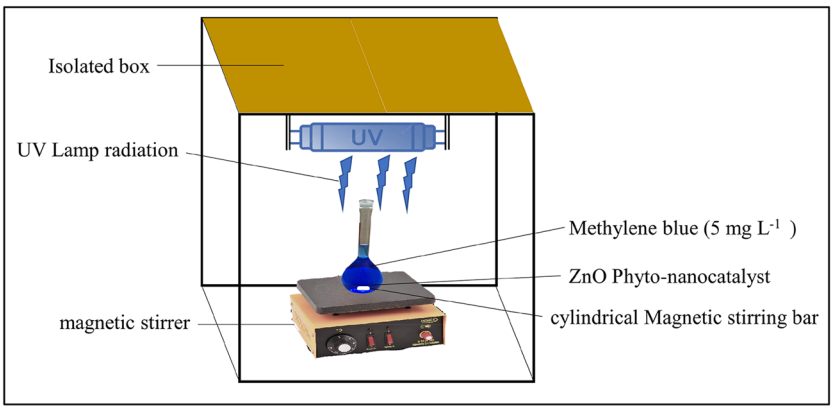

Fig. 2 Schematic of photocatalytic reaction in isolated box

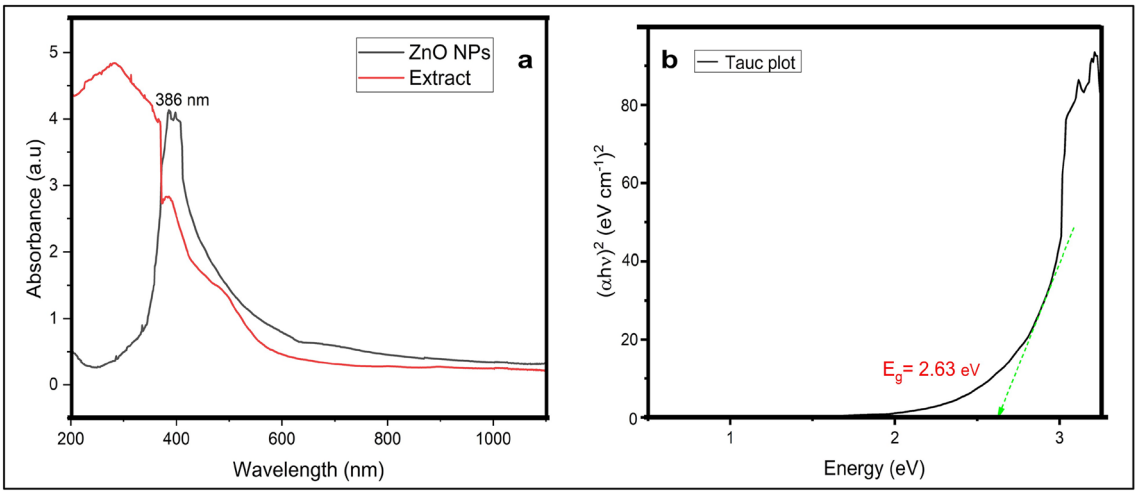

Fig. 3 UV–VIS spectra of *C. oxyacantha* leaf extract and ZnO NPs (**a**). Tauc's plots for the energy band gap of the ZnO NPs (**b**)

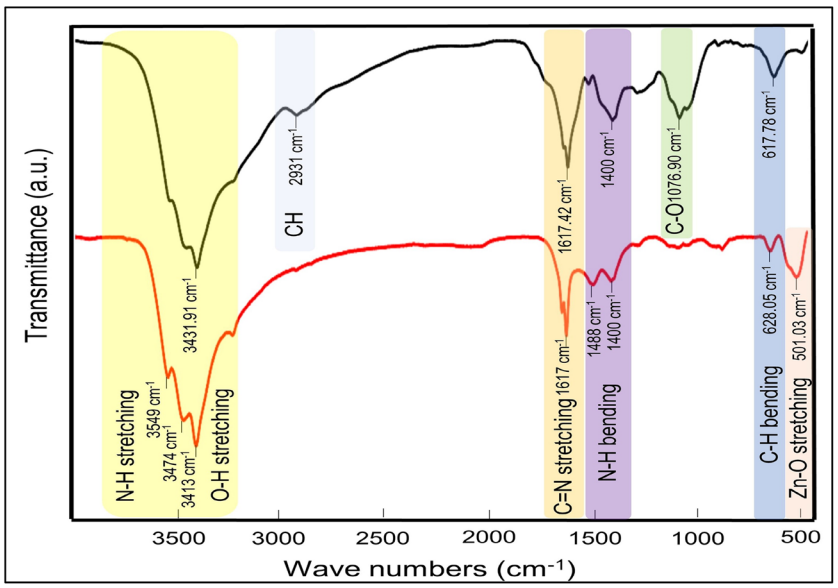

Fig. 4 The FT-IR spectrum of *C. oxyacantha* leaf extract (black) and biosynthesized ZnO NPs (red)

which demonstrate that the antioxidant activity mostly relies on ZnO NP properties.

In the present study, antioxidant activity of *C. oxyacantha* leaf extract and biosynthesized ZnO NPs was assessed by DPPH test. In the DPPH method, a reaction between antioxidant and unstable DPPH* (deep violet color) occurs, subsequently alter into 2,2-diphenyl-2-picrylhydrazine (DPPH:H) with discoloration (light yellow color) (Fig. 8) [38, 50].

As shown in Fig. 9, the radical scavenging activity of ZnO NPs, *C. oxyacantha* leaf extract and a positive sample control, ascorbic acid, was analyzed in various concentrations. While the biosynthesized nanoparticle exhibits high radical scavenging activity (RSA), the leaf extract is poor in that of. It can be derived that the combination of zinc oxide nanoparticles and biomolecules together causes strong antioxidant activity that from the lowest concentration to 200 µg mL^{-1} is premiere than ascorbic acid. To ensure reproducibility, the radical scavenging test was repeated with similar concentrations.

As one of the most reliable mechanisms of nanoparticle cytotoxicity, they generate reactive oxygen species (ROS) that cause oxidative stress [51]. Moreover, various underlying mechanism have been presented for pro-oxidative activeness of nanomaterials. For instance, pro-oxidative metal ions attendance gives the ability to the nanostructures to create ROS by reacting with molecular oxygen. Other mechanism demonstrate that an accumulation of adsorbed nanoparticles may result in structural changes

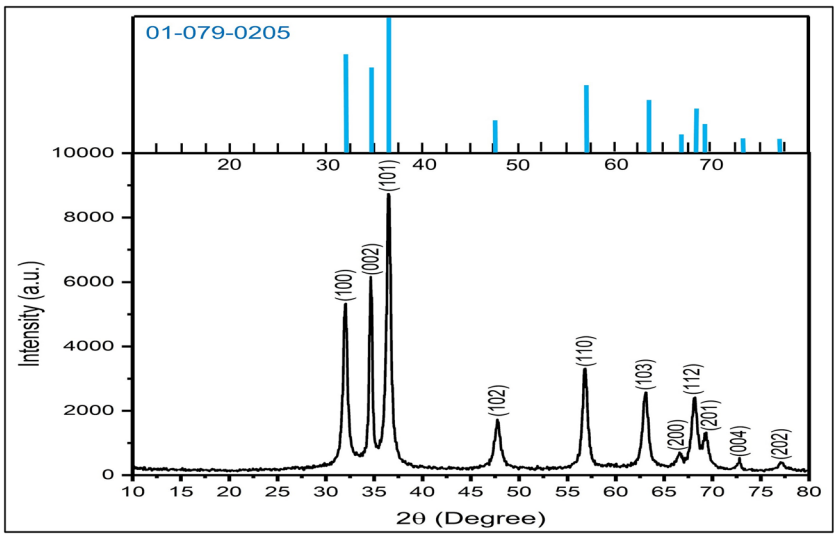

Fig. 5 X-ray diffraction (XRD) crystallography of biosynthesized ZnO NPs

of the cell organ appeared with the reactive oxygen species (ROS) generation. The antioxidant activity of nanoparticles relies on their morphological properties. Nanoparticle size, as a primary factor determining their properties, significantly impacts their antioxidant activity. It has been found that samples of ZnO NPs with the smallest particle size exhibit the highest radical scavenging activity [45], as the biosynthesized ZnO NPs in present study with average size of 26.68 nm does.

3.2.2 Antifungal Activity

Well diffusion and minimum inhibition concentration (MIC) test were quantitatively assessed for *C. oxyacantha* mediated ZnO NPs and leaf extract against *Aspergillus niger* (ATCC 9029) and *Aspergillus brasiliensis* (ATCC 16404). Different concentrations (2, 1, 0.5, 0.25, 0.125, 0.0625, and 0.031 mg mL^{-1}) of ZnO NPs and leaf extract were assessed in MIC test. As shown in Fig. 10 and Table 2, *C. oxyacantha* leaf extract could not inhibit *A. niger* and neither *A. brasiliensis* at any concentration. Thus, the leaf extract does not demonstrate any antifungal activity. In contrast, ZnO NPs inhibit *A. niger* and neither *A. brasiliensis* at 500 µg mL^{-1} and 1000 µg mL^{-1}, respectively.

Based on the results of the MIC study, the synthesized nanoparticles were shown to be effective in inhibiting fungi growth. By using well diffusion technique, the zone of inhibition (ZOI) against *A. niger* and neither *A. brasiliensis* was measured (Fig. 11 and Table 2). The biosynthesized nanoparticle could inhibit both fungi, while the leaf extract didn't display any antimicrobial property. The zone was 14 ± 0.2 mm and 18 ± 0.2 mm for *A. brasiliensis* and *A. niger*, respectively.

The mechanism of antimicrobial activity of ZnO nanoparticles is essentially based on the interaction with the microbial velum, which results in the rupture of the membrane, lead to the fungal cytoplasm leak. Nanoscale ZnO particles can have antimicrobial properties due to oxidative stress caused by reactive oxygen species (ROS) produced on their surfaces that rupture fungi membranes. Reactive oxygen species comprise molecules including oxygen, per hydroxyl radicals, superoxide anion, and hydroxyl radical with ability of destructing DNA, RNA, and oxidize proteins and lipids, therewith resulting the fungi disintegration (Fig. 12) [51–53]. To ensure reproducibility, the antifungal property test was repeated once again under the same conditions and the same results were obtained.

3.3 Catalytic Applications of C. oxyacantha-Mediated ZnO NPs

3.3.1 *Dye Reduction by $NaBH_4$*

The organic dye elimination activity of biosynthesized ZnO NPs was studied by two different approaches. In the first reaction, utilizing the reducing agent $NaBH_4$ and the UV–VIS Spectrophotometer as a monitoring system, Methylene Blue has been reduced to leucomethylene blue (Fig. 13). In spite of the fact that the reaction can easily be monitored by the color change of MB solution, UV–VIS spectrum tracking of each minute of the solution, demonstrated that the degradation was completed in just five minutes (Fig. 14a).

To assure the nanocatalyst efficacy in degradation of MB, two different samples in presence and absence of ZnO NPs were studied. As shown in Fig. 14b. $NaBH_4$ does not demonstrate any catalytic activity on MB; in contrast, in the presence of ZnO NPs, MB was successfully degraded. Additionally, different PH values, temperature

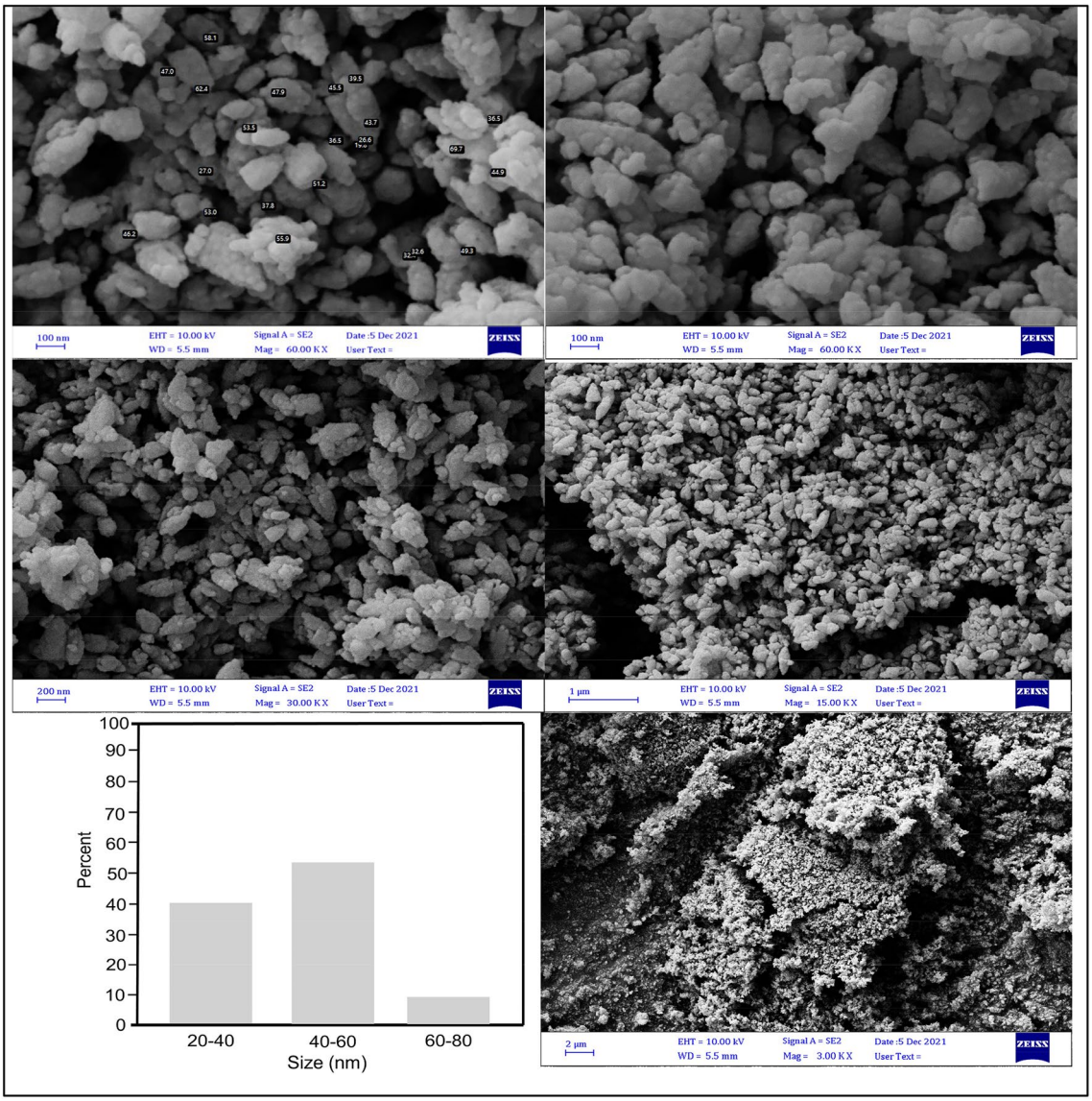

Fig. 6 Scanning electron microscope (SEM) image of biosynthesized ZnO NPs

change effect, and various concentration of ZnO NPs were examined to find the optimal chemical condition for the catalytic reaction. It was observed that ZnO NPs have superior catalytic activity when PH increases. In other word, at the highest PH (pH = 12) ZnO nanocatalyst show their premiere catalytic properties (Fig. 14c). Considering dye wastewaters are often at higher temperatures than other wastewater effluents, the catalytic activity of biosynthesized ZnO NPs was assessed at different temperatures ranging from 15 to 60 °C. As Fig. 14d shows the dye degradation activity of ZnO nanocatalyst slightly increases with temperature rise. nonetheless, ZnO NPs exhibit remarkable organic dye reduction activity at room temperature. To find out the most optimal concentration of ZnO NPs in dye degradation, different concentrations (20, 40, 60, 80, and 100 mg) of the nanocatalyst were examined in present study with no change in dye concentration and PH. As Fig. 14e shows, ZnO NPs in 20 and 40 mg concentrations demonstrate low catalytic activity. on the contrary, at higher dosage (80 and 100 mg) shows high dye degradation activity. Thus, 100 mg concentration was selected as optimum dosage of ZnO NPs.

Using a catalyst in large quantities requires both high activity and stability. To determine the efficiency of their recycling, the ZnO nanoparticles were re-used to degrade MB for six consecutive cycles based on their high catalytic activity (Fig. 14f). The catalytic activity was not significantly diminished after successive degradation rounds.

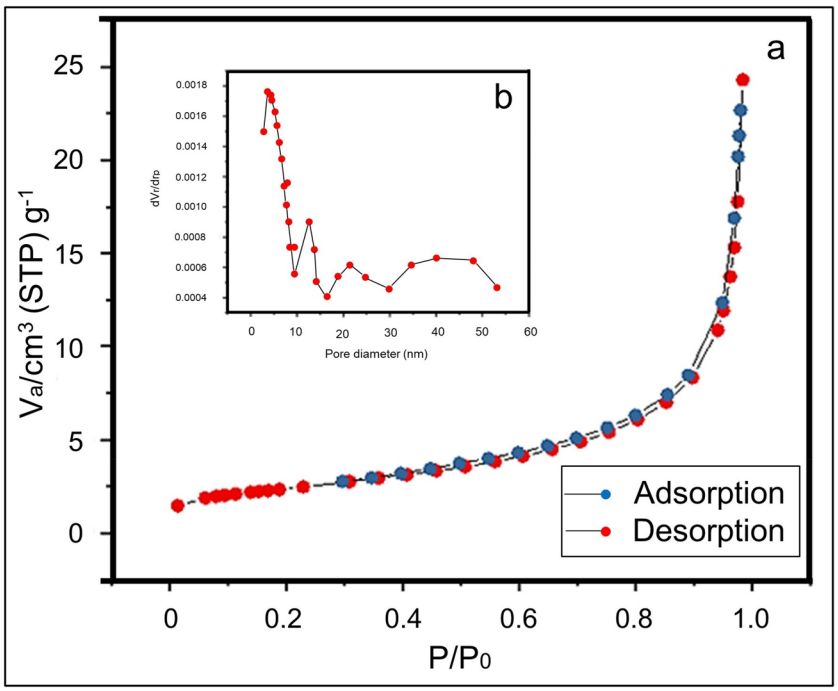

Fig. 7 Nitrogen adsorption/desorption isotherms (**a**) and pore size distribution (**b**) of biosynthesized ZnO NPs

Table 1 BET analysis of ZnO NPs

Sample	S_{BET} (m^2/g)	Total pore volume (cm^3/g)	Average pore diameter (nm)
ZnO	8.65	0.0376	17.40

3.3.2 Dye Reduction by Photocatalytic Reaction

Biosynthesized ZnO NPs have been studied for their photocatalytic activity in various conditions varying the PH level, the nanocatalyst concentration and the temperature. As shown in Fig. 15a, ZnO NPs exhibit remarkable photocatalytic activity in the optimum concentration. To estimate any potential catalytic activity of the UV radiation, two different MB solution in absence and presence of ZnO NPs were studied. It was observed that passing over 20 min the MB solution concentration did not vary in the absence of ZnO (Fig. 15b). As the third part of the study, different thermal conditions were exerted in the isolated box. In contrast to previous reactions with $NaBH_4$, ZnO NPs showed high photocatalytic activity despite low temperatures, although their photocatalytic activity increased with temperature (Fig. 15c). It can be derived that $BH4^-$ ions are more dependent to temperature change. The ZnO NPs photocatalytic characteristic will increase in higher PH value. Figure 15d shows that in acidic values fewer amount of MB dye can be reduced by ZnO nanocatalyst. It is mostly related to the amount of OH* in the reaction medium, that enhance the photodegradation of organic basic dye. On the other

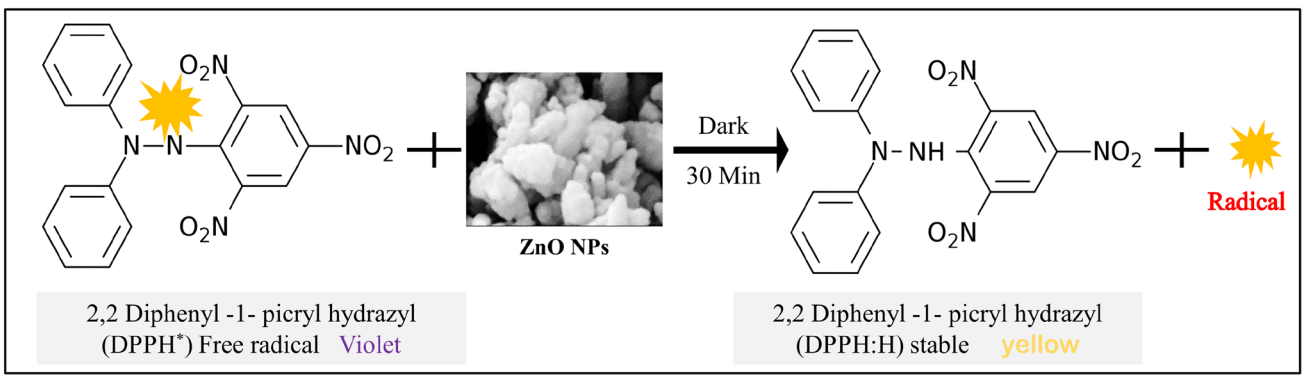

Fig. 8 Radical scavenging reaction by ZnO NPs

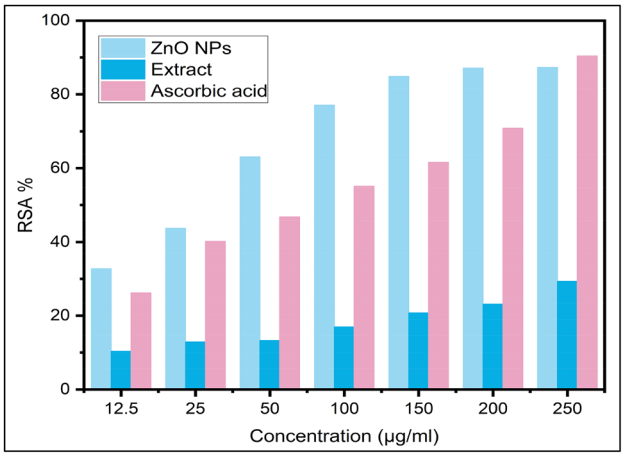

Fig. 9 Comparison between DPPH scavenging activity of ZnO NPs, *C. oxyacantha* leaf extract, and ascorbic acid

hand, higher PH value leads to formation of more negative charges on the photocatalyst surface [54].

For the purpose of illustrating the most optimal concentration of nanocatalyst in photocatalytic reaction, various samples containing 20, 40, 60, 80, and 100 mg ZnO nanocatalyst were radiated under UV lamp in isolated box while dye concentration and pH 7 remained unaltered. It was found that 100 mg of nanocatalyst was the optimal concentration, same as the catalytic reaction in the previous section (Fig. 14e). It can be concluded that the removal of MB dye is considerably influenced by the photocatalyst amount. Higher concentration results in an immense number of active sites in the medium, which will generate more radical ions and enhance the degradation. To estimate photocatalyst recyclability of ZnO NPs, in 6 successive reactions, which nanocatalyst was only washed and dehumidified, the efficiency of them was studied. ZnO NPs could successfully degrade MB after each reaction without any decrement in their photocatalytic property (Fig. 15f).

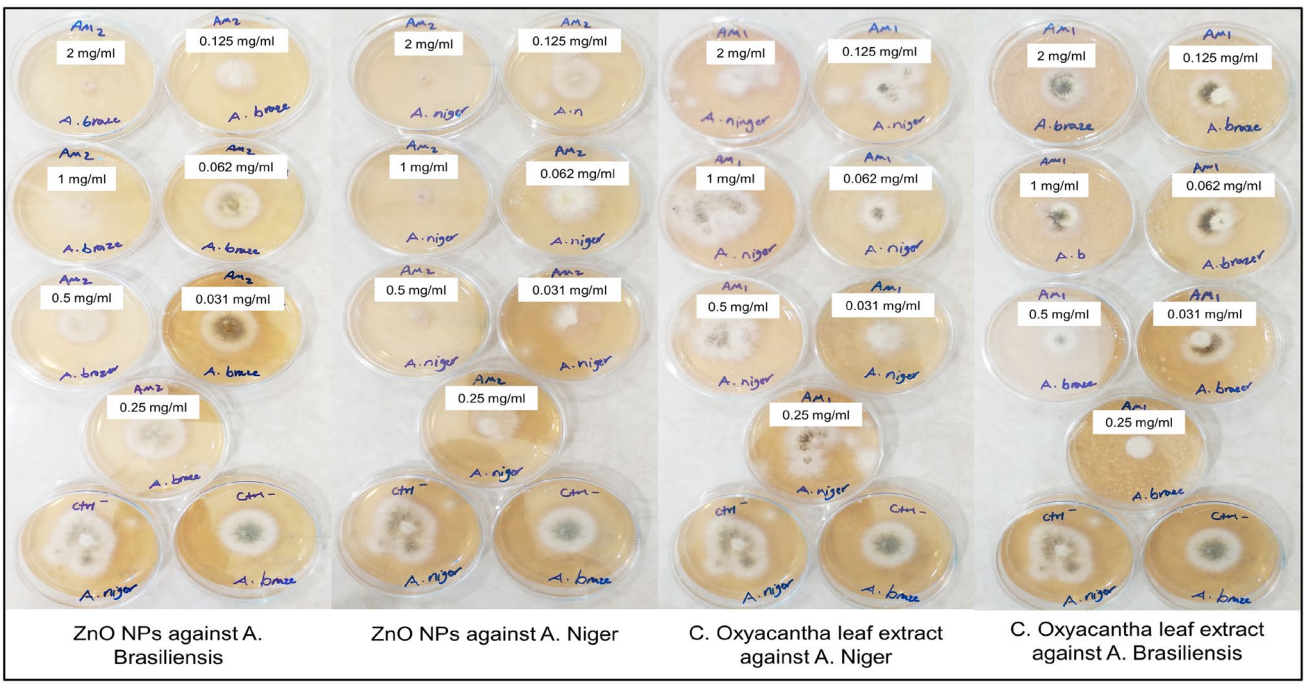

Fig. 10 Minimum inhibition concentration assay of biosynthesized ZnO NPs and *C. oxyacantha* leaf extract

Table 2 Antifungal assessment of ZnO NPs and C. oxyacantha leaf extract

Microorganism	Sample				Control	
	ZnO NPs		*C. oxyacantha* leaf extract		Nystatin	
	ZOI (mm)	MIC (µg mL^{-1})	ZOI (mm)	MIC (µg mL^{-1})	ZOI (mm)	MIC (µg mL^{-1})
A. brasiliensis	14 ± 0.2	1000	-	> 2000	27 ± 0.2	31.2
A. niger	18 ± 0.2	500	-	> 2000	30 ± 0.2	31.2

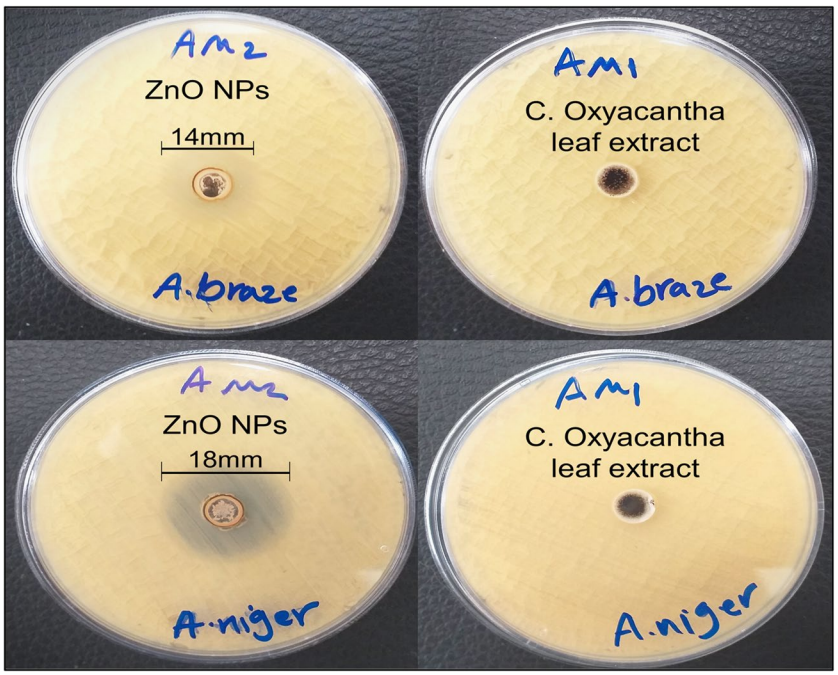

Fig. 11 Well diffusion test of ZnO NPs and *C. oxyacantha* leaf extract

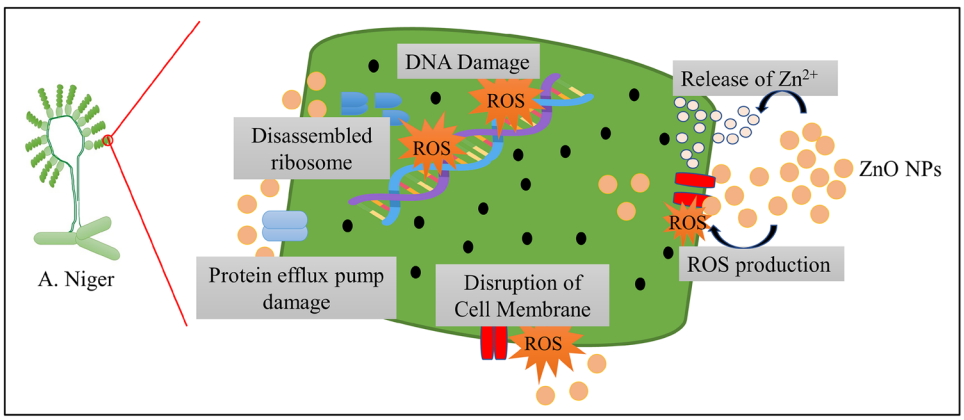

Fig. 12 Antifungal mechanism of ZnO NPs

Since some photocatalytic tests are conducted under sunlight, and due to its economics, sunlight is preferred over UV light for wastewater treatment, we decided to evaluate ZnO nanocatalyst's photodegradation potential as such. The same amount of ZnO NPs (100 mg) with the same concentration of MB solution was used in this study. While the intensity of light determines the amount of energy input into a photocatalytic process, upon landing more radiation on the catalyst surface, more hydroxyl radicals are formed, increasing degradation efficiency. During the experimentation period, the average solar irradiance was 477 W/m^2. Following the same reaction conditions, the pollutant removal efficiency was measured. Figure 16 shows that the solar base photodegradation process is much slower than that of UV light.

It was observed that after 5-min radiation of sunlight to MB solution containing ZnO nanocatalyst, only 25% of MB was reduced. While in the same time 75% MB was reduced by UV lamp radiation. Passing 20 min of both UV and sunlight radiation, pollutant removal increased 98% and 52%, respectively. Following the reaction after 30 min UV degraded MB was 100% treated, while sunlight degraded MB 69%. Finally, MB dye reduced over 90% after 50 min under direct radiation of sunlight. As a result, it can be concluded that solar photocatalytic degradation is efficient in regions with high solar light levels, reducing energy costs and making it more environmentally friendly. The photocatalytic repercussion mechanism stats while the electrons (e-) in the valence band (VB) of the ZnO semiconductor absorb the photons after having received the adequate energy from the light source. The photoexcited electrons will jump towards the ZnO conductor band (CB) and leave a positive charged hole (h+) in the (VB).

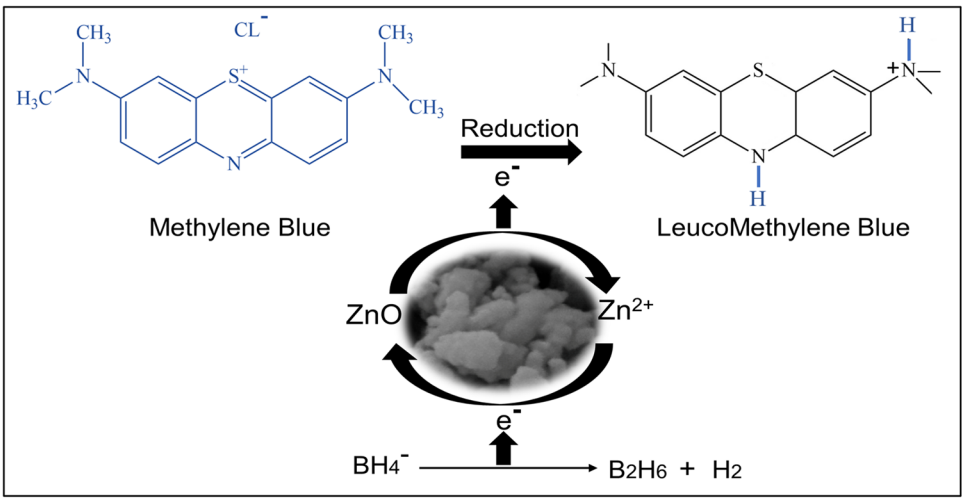

Fig. 13 MB degradation mechanism by ZnO NPs and $NaBH_4$

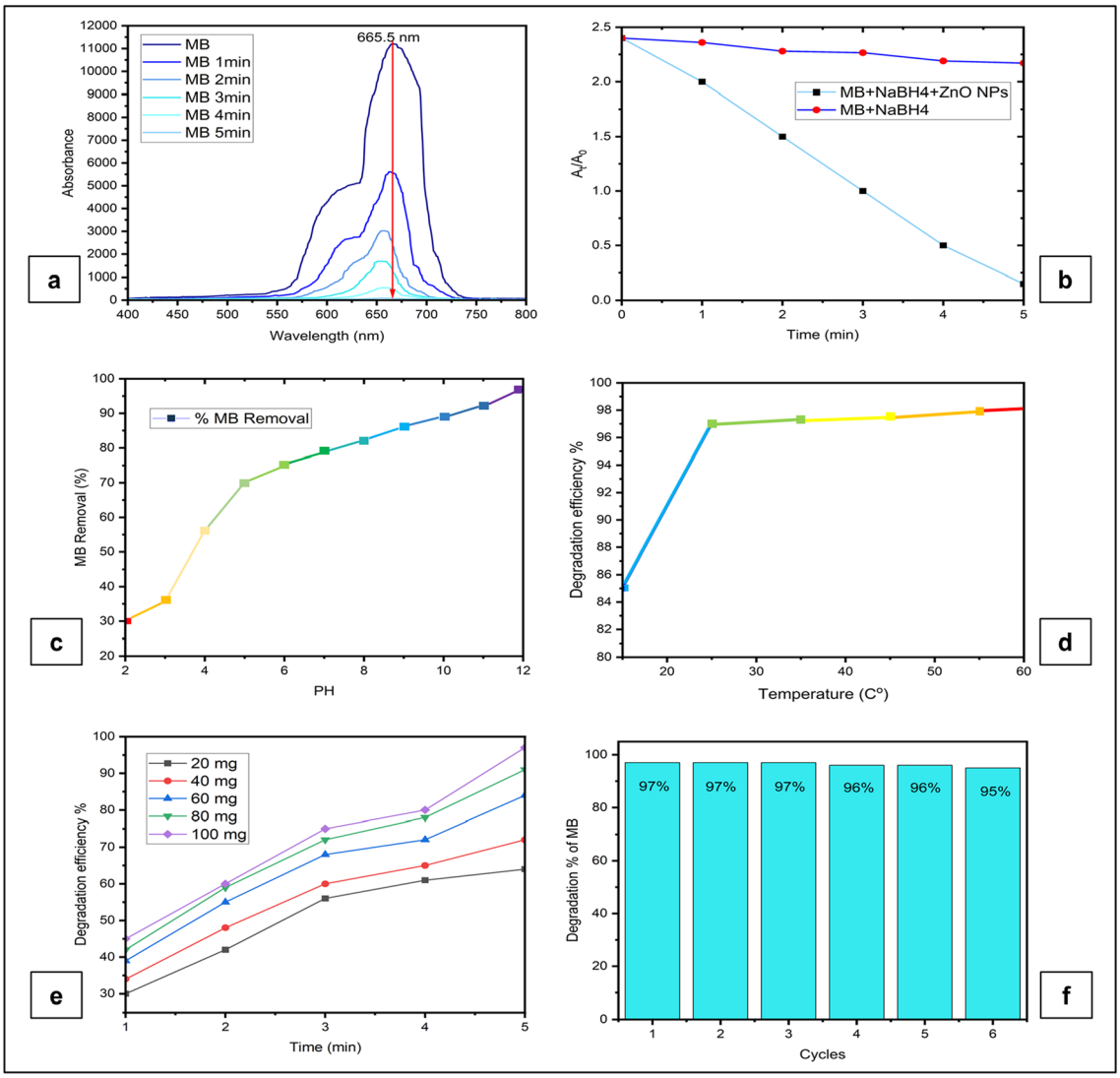

Fig. 14 Successive reduction of MB by ZnO NPs (**a**). Dye reduction in presence and absence of ZnO NPs (**b**). PH effect on ZnO NPs catalytic activity (**c**). Temperature effect on ZnO NP catalytic activity (**d**). Concentration effect on MB degradation activity of ZnO NPs (**e**). Recyclability of ZnO NPs in MB degradation (**f**)

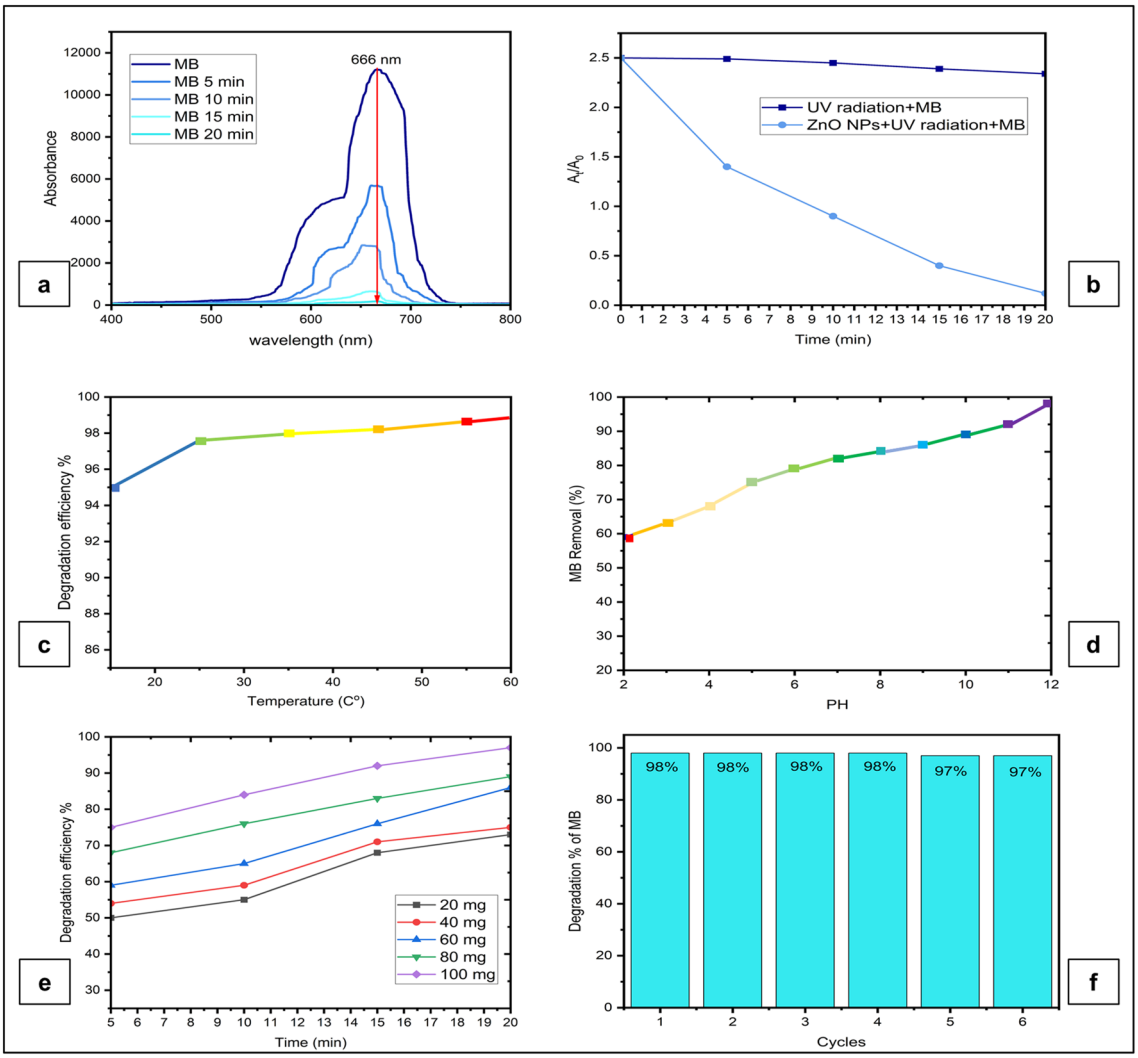

Fig. 15 Successive photodegradation of MB by ZnO NPs and UV lamp (185 nm) (**a**). Effect of presence of nanocatalyst in reaction (**b**). Thermal change effect on photocatalytic activity of ZnO NPs (**c**). PH increment effect on photocatalytic activity of ZnO NPs (**d**). Optimal concentration assessment of ZnO photocatalyst (**e**). Photocatalyst recyclability of ZnO NPs (**f**)

The manufactured electron–hole pairs (e^-/h^+) afterward reacts with water and oxygen to create reactive oxygen species specially hydroxyl radicals and superoxide anions. The produced free radicals act as intense oxidizing agents, which subsequently act reciprocally with the contaminants, fracturing their chemical linkage, leading to total mineralization (Fig. 17).

3.3.3 Suzuki Cross-Coupling Reaction by ZnO Photocatalyst

Free palladium Suzuki coupling of iodobenzene with phenylboronic acid leaded to facile and inexpensive synthesis of biphenyl (Fig. 18). Thus, the ZnO NPs are able to photocatalysis the Suzuki reaction in absence of any other catalyst, including Pd. 90% yield was achieved with the product, a white solid in 15 min. The melting point of product was 66.7 °C. IR (KBr, cm-1): 1710, 1684, 1616, 845; 1H-NMR 7.590–7.570 (m, 4H), 7.450–7.400 (m, 4H), 7.350–7.300 (m, 2H); 13C-NMR 141.24, 128.74, 127.24, 127.16, 77.32, 77.21, 76.69.

We developed an efficient and ligand-free Suzuki coupling reaction protocol in water under LED light using ZnO NPs as a photocatalyst, K_2CO_3 as a base, and polyethylene glycol as an additive. To study the photocatalyst recyclability of ZnO NPs, four continuous reaction was performed. Same concentration of ZnO NPs (5 mg) and unaltered coupling reaction was used in all cycles. In terms of reaction productivity, no significant changes were observed. It can be derived that the biosynthesized ZnO NPs demonstrate remarkable catalytic property in low dosage with no decline

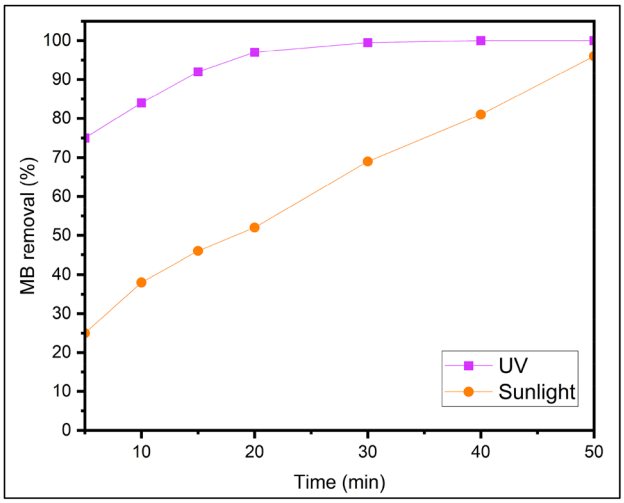

Fig. 16 Comparison of UV radiation with sunlight in photodegradation of MB

in activity after four reaction cycle. Suzuki cross-coupling reactions are usually performed by Pd NPs by lengthy process, but the present study shows that ZnO photo-nanocatalysts can speed up the reaction.

4 Conclusion

This study is the first to show that *C. oxyacantha* leaf extract can be used as an effective reduction/oxidizing chemical agent for the biosynthesis of spherical ZnO NPs with high catalytic activity. As FE-SEM images and XRD analysis exhibited, these nanoparticles have average size of 26.68 nm, which result in their high antioxidant activity. On the other hand, these nanoparticles are highly potent in MB dye degradation both using $NaBH_4$ and UV lamp. Also, these nanoparticles catalyze dye reduction under sunlight, taking longer than UV lamps to complete the reaction. It was found that 100 mg of ZnO NPs can reduce MB over 97% in 5 and 20 min as a catalyst and photocatalyst. As a multi-functional nanoscale compound, ZnO acts as a potent antioxidant and antifungal. Using the radical scavenging test, DPPH, 200 µg mL^{-1} of ZnO nanoparticles showed higher antioxidant activity than ascorbic acid as the control sample. Finally, these green synthesized nanoparticles for the first time photocatalyzed the Suzuki coupling reaction effectually, producing 90% biphenyl yield. As a result, *C. oxyacantha* leaf extract gives ZnO nanoparticles unique morphological properties and efficiency, and

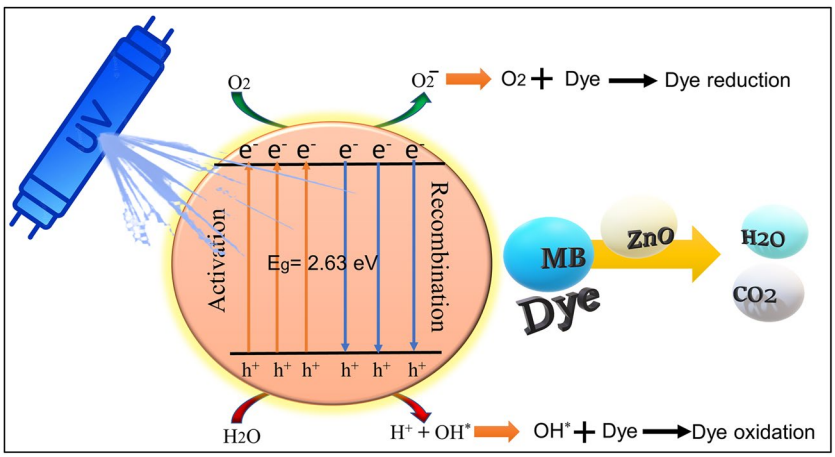

Fig. 17 Dye degradation mechanism of ZnO NPs

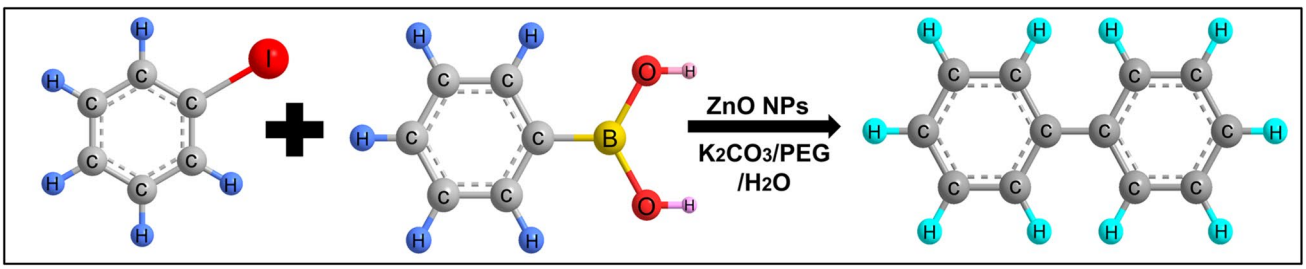

Fig. 18 Synthesis of biphenyl by ZnO photocatalyst

these nanoparticles can compete with other nanoparticles fabricated by other methods.

Acknowledgements The authors are thankful to the Department of Chemistry of Qom University of Technology for technical support in this project.

Author Contribution The manuscript was written through contributions of Alireza Momeni, Mohammad Hadi Meshkatalsadat and Behjat Pouramiri. Authors have given approval to the final version of the manuscript.

Data Availability The authors confirm that the data supporting the findings of this study are available within the article. Also, on request, the corresponding author can provide the raw data obtained from all tests that were used to draw plots.

Declarations

Competing Interests The authors declare no competing interests.

Conflict of Interest The authors declare no competing interests.

Ethical Approval A full ethical approval was given by the Ethics Committee of Qom university of technology. In addition, this material is the authors' own original work, which has not been previously published elsewhere.

Consent to Participate Additional informed consent was obtained from all individual participants for whom identifying information is included in this article.

Consent to Publish All authors declare their consent for the publication of all details, which can include photographs, plots, and texts within the ("manuscript") to be published in the Journal of Environmental Science and Pollution Research.

References

1. Vasantharaj, S., Sathiyavimal, S., Senthilkumar, P., Kalpana, V. N., Rajalakshmi, G., Alsehli, M., Elfasakhany, A., & Pugazhendhi, A. (2021). Enhanced photocatalytic degradation of water pollutants using bio-green synthesis of zinc oxide nanoparticles (ZnO NPs). *Journal of Environmental Chemical Engineering, 9*, 105772. https://doi.org/10.1016/j.jece.2021.105772
2. Rajendrachari, S., Taslimi, P., Karaoglanli, A. C., Uzun, O., Alp, E., & Jayaprakash, G. K. (2021). Photocatalytic degradation of Rhodamine B (RhB) dye in waste water and enzymatic inhibition study using cauliflower shaped ZnO nanoparticles synthesized by a novel One-pot green synthesis method. *Arabian Journal of Chemistry, 14*, 103180. https://doi.org/10.1016/j.arabjc.2021.103180
3. Iqbal, Y., Raouf Malik, A., Iqbal, T., Hammad Aziz, M., Ahmed, F., Abolaban, F. A., Mansoor Ali, S., & Ullah, H. (2021). Green synthesis of ZnO and Ag-doped ZnO nanoparticles using Azadirachta indica leaves: Characterization and their potential antibacterial, antidiabetic, and wound-healing activities. *Materials Letters., 305*, 130671. https://doi.org/10.1016/j.matlet.2021.130671
4. Meyers, M. A., Mishra, A., & Benson, D. J. (2006). Mechanical properties of nanocrystalline materials. *Progress in Materials Science., 51*, 427–556. https://doi.org/10.1016/j.pmatsci.2005.08.003
5. Singh, J. P. (2020). Bottom-up and top-down approaches for MgO. *IntechOpen*. https://doi.org/10.5772/intechopen.91182
6. Sepeur, S. (2008). *Nanotechnology: technical basics and applications.* Vincentz Network GmbH & Co KG.
7. Jiang, J., Oberdörster, G., & Biswas, P. (2009). Characterization of size, surface charge, and agglomeration state of nanoparticle dispersions for toxicological studies. *Journal of Nanoparticle Research., 11*, 77–89. https://doi.org/10.1007/s11051-008-9446-4
8. Duran, N., Marcato, P., Souza, G., Alves, O., & Esposito, E. (2007). Antibacterial effect of silver nanoparticles produced by fungal process on textile fabrics and their effluent treatment. *Journal of Biomedical Nanotechnology., 3*, 203–208. https://doi.org/10.1166/jbn.2007.022
9. Habbal, O., Hasson, S. S., El-Hag, A. H., Al-Mahrooqi, Z., Al-Hashmi, N., Al-Bimani, Z., Al-Balushi, M. S., & Al-Jabri, A. A. (2011). Antibacterial activity of Lawsonia inermis Linn (Henna) against Pseudomonas aeruginosa. *Asian Pacific Journal of Tropical Biomedicine, 1*, 173–176. https://doi.org/10.1016/s2221-1691(11)60021-x
10. Yuvakkumar, R., Suresh, J., Nathanael, A. J., Sundrarajan, M., & Hong, S. I. (2014). Novel green synthetic strategy to prepare ZnO nanocrystals using rambutan (Nephelium lappaceum L.) peel extract and its antibacterial applications. *Materials Science & Engineering, C: Materials for Biological Applications, 41*, 17–27. https://doi.org/10.1016/j.msec.2014.04.025
11. Qu, J., Yuan, X., Wang, X., & Shao, P. (2011). Zinc accumulation and synthesis of ZnO nanoparticles using Physalis alkekengi L. *Environmental Pollution, 159*, 1783–1788. https://doi.org/10.1016/j.envpol.2011.04.016
12. Ramesh, P., Saravanan, K., Manogar, P., Johnson, J., Vinoth, E., & Mayakannan, M. (2021). Green synthesis and characterization of biocompatible zinc oxide nanoparticles and evaluation of its antibacterial potential. *Sensing and Bio-Sensing Research, 31*, 100399. https://doi.org/10.1016/j.sbsr.2021.100399
13. Shahein, M. R., Atwaa, E. S. H., Babalghith, A. O., Alrashdi, B. M., Radwan, H. A., Umair, M., ... & Elmahallawy, E. K. (2022). Impact of incorporating the aqueous extract of hawthorn (C. oxyanatha) leaves on yogurt properties and its therapeutic effects against oxidative stress induced by carbon tetrachloride in rats. *Fermentation, 8*(5), 200. https://doi.org/10.3390/fermentation8050200
14. Benabderrahmane, W., Lores, M., Benaissa, O., Lamas, J. P., de Miguel, T., Amrani, A., Benayache, F., & Benayache, S. (2021). Polyphenolic content and bioactivities of Crataegus oxyacantha L. (Rosaceae). *Natural product research., 35*, 627–632.
15. Gautam, A. K., Avasthi, S., & Bhadauria, R. (2011). Diversity, pathogenicity and toxicology of A. niger: An important spoilage fungi. *Research Journal of Microbiology, 6*, 270–280. https://doi.org/10.3923/jm.2011.270.280
16. Schuster, E., Dunn-Coleman, N., Frisvad, J., & van Dijck, P. (2002). On the safety of Aspergillus niger – A review. *Applied Microbiology and Biotechnology., 59*, 426–435. https://doi.org/10.1007/s00253-002-1032-6
17. Perfect, J. R., Cox, G. M., Lee, J. Y., Kauffman, C. A., de Repentigny, L., Chapman, S. W., Morrison, V. A., Pappas, P., Hiemenz, J. W., & Stevens, D. A. (2001). The impact of culture isolation of Aspergillus species: A hospital-based survey of aspergillosis. *Clinical Infectious Diseases, 33*, 1824–1833. https://doi.org/10.1086/323900
18. Patterson, T. F. (2016). Practice guidelines for the diagnosis and management of aspergillosis. *Clinical Infectious Diseases., 63*, 1–60.
19. Pillai, A. M., Sivasankarapillai, V. S., Rahdar, A., Joseph, J., Sadeghfar, F., Rajesh, K., & Kyzas, G. Z. (2020). Green synthesis and characterization of zinc oxide nanoparticles with antibacterial and antifungal activity. *Journal of Molecular Structure, 1211*, 128107.
20. Avalos, A., Haza, A. I., Mateo, D., & Morales, P. (2014). Cytotoxicity and ROS production of manufactured silver nanoparticles of different sizes in hepatoma and leukemia cells. *Journal of applied toxicology., 34*, 413–423.

21. Rehana, D., Mahendiran, D., Kumar, R. S., & Rahiman, A. K. (2017). In vitro antioxidant and antidiabetic activities of zinc oxide nanoparticles synthesized using different plant extracts. *Bioprocess and biosystems engineering., 40*, 943–957.
22. Kerr, M. E., Bender, C. M., & Monti, E. J. (1996). An introduction to oxygen free radicals. *Heart & Lung: the Journal of Critical Care, 25*(3), 200–209. https://doi.org/10.1016/s0147-9563(96)80030-6
23. Narayan, N., Meiyazhagan, A., & Vajtai, R. (2019). *Metal nanoparticles as green catalysts. Materials., 12*, 3602.
24. Prajapati, P. K., Saini, S., & Jain, S. L. (2020). Nickel mediated palladium free photocatalytic Suzuki-coupling reaction under visible light irradiation. *Journal of Materials Chemistry A., 8*, 5246–5254.
25. Habibi, M. H., & Rezvani, Z. (2015). Photocatalytic degradation of an azo textile dye (CI Reactive Red 195 (3BF)) in aqueous solution over copper cobaltite nanocomposite coated on glass by Doctor Blade method. *Spectrochimica Acta Part A: Molecular and Biomolecular Spectroscopy., 147*, 173–177.
26. Padhi, B. (2012). Pollution due to synthetic dyes toxicity & carcinogenicity studies and remediation. *International journal of environmental sciences., 3*, 940–955.
27. Schirmer, R. H., Adler, H., Pickhardt, M., & Mandelkow, E. (2011). Lest we forget you—methylene blue….*Neurobiology of aging, 32*(12), 2325.e7–2325.e16. https://doi.org/10.1016/j.neurobiolaging.2010.12.012
28. Khan, I., Saeed, K., Zekker, I., Zhang, B., Hendi, A. H., Ahmad, A., Ahmad, S., Zada, N., Ahmad, H., & Shah, L. A. (2022). Review on methylene blue: Its properties, uses, toxicity and photodegradation. *Water, 14*, 242.
29. Santoso, E., Ediati, R., Kusumawati, Y., Bahruji, H., Sulistiono, D., & Prasetyoko, D. (2020). Review on recent advances of carbon based adsorbent for methylene blue removal from waste water. *Materials Today Chemistry, 16*, 100233.
30. Zhou, S., Du, Z., Li, X., Zhang, Y., He, Y., & Zhang, Y. (2019). Degradation of methylene blue by natural manganese oxides: Kinetics and transformation products. *Royal Society open science, 6*, 190351.
31. Singh, J., Dutta, T., Kim, K.-H., Rawat, M., Samddar, P., & Kumar, P. (2018). 'Green'synthesis of metals and their oxide nanoparticles: Applications for environmental remediation. *Journal of nanobiotechnology., 16*, 1–24.
32. Qumar, U., Hassan, J. Z., Bhatti, R. A., Raza, A., Nazir, G., Nabgan, W., & Ikram, M. (2022). Photocatalysis vs adsorption by metal oxide nanoparticles. *Journal of Materials Science & Technology, 131*, 122–166. https://doi.org/10.1016/j.jmst.2022.05.020
33. Khademalrasool, M., & Farbod, M. (2016). Preparation of ZnO nanoparticles/Ag nanowires nanocomposites as plasmonic photocatalysts and investigation of the effect of concentration and diameter size of Ag nanowires on their photocatalytic performance. *Journal of Alloys and Compounds., 664*, 707–714.
34. Lee, K. M., Lai, C. W., Ngai, K. S., & Juan, J. C. (2016). Recent developments of zinc oxide based photocatalyst in water treatment technology: A review. *Water research., 88*, 428–448.
35. Abbas, K. N., & Bidin, N. (2017). Morphological driven photocatalytic activity of ZnO nanostructures. *Applied Surface Science., 394*, 498–508.
36. Qi, K., Cheng, B., Yu, J., & Ho, W. (2017). Review on the improvement of the photocatalytic and antibacterial activities of ZnO. *Journal of Alloys and Compounds., 727*, 792–820.
37. Sekhar, E. C., Rao, K. K., Rao, K. M. S., & Alisha, S. B. (2018). A simple biosynthesis of silver nanoparticles from Syzygium cumini stem bark aqueous extract and their spectrochemical and antimicrobial studies. *Journal of Applied Pharmaceutical Science., 8*, 073–079.
38. Du, L., Suo, S., Wang, G., Jia, H., Liu, K. J., Zhao, B., & Liu, Y. (2013). Mechanism and cellular kinetic studies of the enhancement of antioxidant activity by using surface-functionalized gold nanoparticles. *Chemistry A European Journal, 19*, 1281–1287.
39. El-Sharkawy, E. A., Soliman, A. Y., & Al-Amer, K. M. (2007). Comparative study for the removal of methylene blue via adsorption and photocatalytic degradation. *Journal of colloid and interface science, 310*(2), 498–508. https://doi.org/10.1016/j.jcis.2007.02.013
40. Parveen, S., Wani, A. H., Shah, M. A., Devi, H. S., Bhat, M. Y., & Koka, J. A. (2018). Preparation, characterization and antifungal activity of iron oxide nanoparticles. *Microbial pathogenesis., 115*, 287–292.
41 Efafi, B., Ghamsari, M. S., Aberoumand, M., Ara, M. M., Ghamsari, A. S., & Rad, H. H. (2014). Aluminum doped ZnO sol–gel derived nanocrystals: Raman spectroscopy and solid solubility characterization. *Physica status solidi (a), 211*, 2426–2430.
42. Senthilkumar, N., Nandhakumar, E., Priya, P., Soni, D., Vimalan, M., & Potheher, I. V. (2017). Synthesis of ZnO nanoparticles using leaf extract of Tectona grandis (L.) and their anti-bacterial, anti-arthritic, anti-oxidant and in vitro cytotoxicity activities. *New Journal of Chemistry., 41*, 10347–10356.
43. Stan, M., Popa, A., Toloman, D., Silipas, T.-D., & Vodnar, D. C. (2016). Antibacterial and antioxidant activities of ZnO nanoparticles synthesized using extracts of Allium sativum, Rosmarinus officinalis and Ocimum basilicum. *Acta Metallurgica Sinica (English Letters)., 29*, 228–236.
44. Agarwal, H., Kumar, S. V., & Rajeshkumar, S. (2017). A review on green synthesis of zinc oxide nanoparticles–An eco-friendly approach. *Resource-Efficient Technologies., 3*, 406–413.
45. Sundrarajan, M., Ambika, S., & Bharathi, K. (2015). Plant-extract mediated synthesis of ZnO nanoparticles using Pongamia pinnata and their activity against pathogenic bacteria. *Advanced powder technology., 26*, 1294–1299.
46. Halliwell, B. (1995). Antioxidant characterization: methodology and mechanism. *Biochemical pharmacology, 49*(10), 1341–1348. https://doi.org/10.1016/0006-2952(95)00088-H
47. Young, I., & Woodside, J. (2001). Antioxidants in health and disease. *Journal of clinical pathology., 54*, 176–186.
48. Kumar, B., Smita, K., Cumbal, L., & Debut, A. (2014). Green approach for fabrication and applications of zinc oxide nanoparticles. *Bioinorganic Chemistry and Applications., 2014*, 523869. https://doi.org/10.1155/2014/523869
49. Alavi, M., Karimi, N., & Salimikia, I. (2019). Phytosynthesis of zinc oxide nanoparticles and its antibacterial, antiquorum sensing, antimotility, and antioxidant capacities against multidrug resistant bacteria. *Journal of Industrial and Engineering Chemistry., 72*, 457–473.
50. Kumar, B., Smita, K., Cumbal, L., & Debut, A. (2014). Synthesis of silver nanoparticles using Sacha inchi (Plukenetia volubilis L.) leaf extracts. *Saudi journal of biological sciences., 21*, 605–609.
51. Li, M., Zhu, L., & Lin, D. (2011). Toxicity of ZnO nanoparticles to Escherichia coli: Mechanism and the influence of medium components. *Environmental science & technology., 45*, 1977–1983.
52. Zhong, L., Liu, H., Samal, M., & Yun, K. (2018). Synthesis of ZnO nanoparticles-decorated spindle-shaped graphene oxide for application in synergistic antibacterial activity. *Journal of Photochemistry and Photobiology B: Biology., 183*, 293–301.
53. Krishnamoorthy, K., Veerapandian, M., Zhang, L.-H., Yun, K., & Kim, S. J. (2012). Antibacterial efficiency of graphene nanosheets against pathogenic bacteria via lipid peroxidation. *The journal of physical chemistry C., 116*, 17280–17287.
54. Farzana, M. H., & Meenakshi, S. (2014). Synergistic effect of chitosan and titanium dioxide on the removal of toxic dyes by the photodegradation technique. *Industrial & Engineering Chemistry Research., 53*, 55–63.